Scripta Materialia 187 (2020) 13–18

Contents lists available at ScienceDirect

Scripta Materialia

journal homepage: www.elsevier.com/locate/scriptamat

Enhancement of plasticity for FeCoBSiNb bulk metallic glass with superhigh strength through cryogenic thermal cycling

Siyi Di[a], Qianqian Wang[a], Jing Zhou[a], Yiyang Shen[a], Jiaqi Li[a], Mingyun Zhu[b], Kuibo Yin[b], Qiaoshi Zeng[a], Litao Sun[b], Baolong Shen[a,c,*]

[a] School of Materials Science and Engineering, Jiangsu Key Laboratory for Advanced Metallic Materials, Southeast University, Nanjing 211189, China
[b] SEU-FEI Nano-Pico Center, Key Laboratory of MEMS of Ministry of Education, Southeast University, Nanjing 210096, China
[c] Institute of Massive Amorphous Metal Science, China University of Mining and Technology, Xuzhou 221116, China

ARTICLE INFO

Article history:
Received 22 April 2020
Revised 27 May 2020
Accepted 29 May 2020

Keywords:
Bulk metallic glass
Plasticity
Cryogenic thermal cycling
Heterostructures

ABSTRACT

The mechanical properties and atomic-scale structure of the $[(Fe_{0.5}Co_{0.5})_{0.75}B_{0.2}Si_{0.05}]_{96}Nb_4$ bulk metallic glass (BMG) treated with cryogenic thermal cycling were studied. The obtained Fe-based BMG shows an improvement of plastic strain from 1.4 to 6.1% and maintains a high yield strength over 4000 MPa. The high structural disorder degree caused by rejuvenation, as well as the fine-tuned crystal-like ordering structures induced by internal stress, contribute to the formation of multiple shear bands, and thus results in the enhancement of plasticity. This work provides a new insight to develop plastic Fe-based BMGs through modulating atomic-scale structure.

Fe-based bulk metallic glasses (BMGs) have attracted intense attention because of their excellent soft-magnetic properties and superhigh strength, as well as relatively low raw material cost [1–3]. Unfortunately, the negligible plasticity of Fe-based BMGs obstructs their widespread applications as structural and functional materials [2,4]. In the past decades, a series of plastic Fe-based BMGs and BMG matrix composite systems have been developed through composition modification [5–9]. Nevertheless, this method is usually accompanied by sacrificing the strength, soft magnetic properties or glass-forming ability (GFA). Recently, it has been reported that the cryogenic thermal cycling (CTC) treatment, which subjects samples to thermal cycling between ambient temperature and cryogenic temperature, can rejuvenate some BMGs to improve their plasticity [10–12]. Compared with the composition modification, the CTC treatment has no effect on GFA and barely weakens the strength of studied BMGs [11]. Particularly, it has been reported that CTC treatment has little deterioration on soft-magnetic properties of Fe-based metallic glass ribbons [13]. Nevertheless, it is still unclear whether the plasticity of Fe-based BMG can be improved via CTC treatment.

Besides, there is no general consensus on what CTC treatment really does at the structural level. One of the theories is that the internal stress of the BMGs increases during CTC treatment, leading to the formation of a higher concentration of soft spots or flow "defects". This results in the improvement of structural heterogeneities in the amorphous matrix, which causes the increase of plasticity [10]. However, this model may not be a complete description for the atomic-scale structure transformation, because some BMGs had no response and even underwent inferior plasticity after CTC treatment or increased numbers of cycling [14,15].

In this study, the effect of CTC treatment on the mechanical properties of $[(Fe_{0.5}Co_{0.5})_{0.75}B_{0.2}Si_{0.05}]_{96}Nb_4$ BMG was investigated with the aim of increasing its plasticity but maintaining its superhigh strength and large GFA [16]. A significantly improved plastic strain (ε_p) of 6.1% combined with a superhigh yield strength (σ_y) over 4000 MPa was obtained through CTC treatment at appropriate condition. The higher structural disorder degree and more crystal-like ordering (CLO) structures with appropriate size induced by CTC treatment are the reasons for the improvement of plasticity. Besides, the samples treated at other CTC conditions experience decrease of plasticity due to the higher degree of ordering and crystal growth.

Alloy ingots with a nominal atomic composition of $[(Fe_{0.5}Co_{0.5})_{0.75}B_{0.2}Si_{0.05}]_{96}Nb_4$ were prepared by induction melting high-purity (> 99.9 wt.%) constituents under a high-purified argon atmosphere. Cylindrical BMG samples with a diameter of 1 mm were fabricated by copper mold casting. During the CTC treatment, the as-prepared $[(Fe_{0.5}Co_{0.5})_{0.75}B_{0.2}Si_{0.05}]_{96}Nb_4$ BMG samples were firstly dipped into liquid nitrogen for 1 min, then immersed in silicone oil (Polydimethylsiloxane, supplied by Dow Corning) at 433, 473, 513, 533, and 563 K (0.52–0.68 of the glass

* Corresponding author.
E-mail address: blshen@seu.edu.cn (B. Shen).

https://doi.org/10.1016/j.scriptamat.2020.05.059
1359-6462/

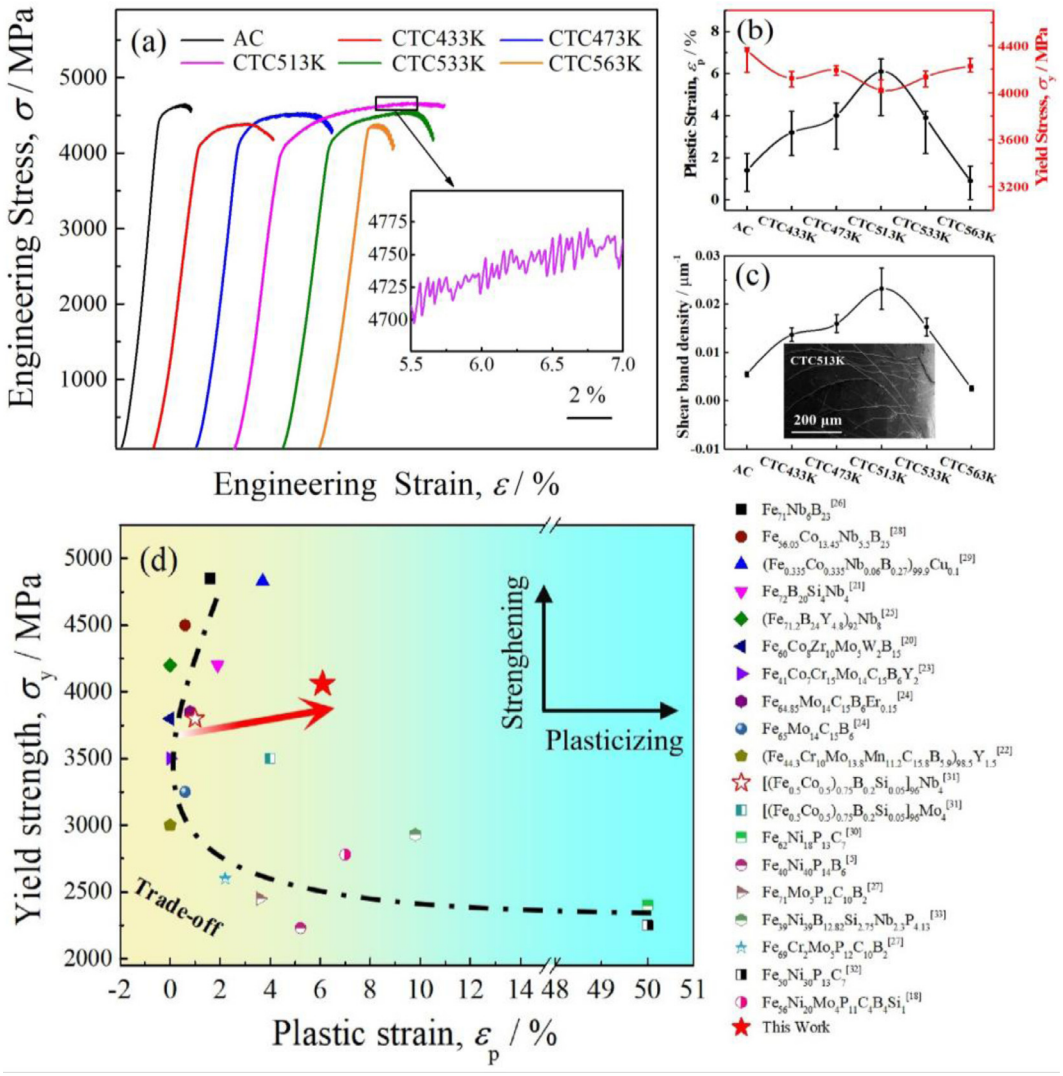

Fig. 1. (a) The representative engineering stress-strain curves of the AC and CTC treated $[(Fe_{0.5}Co_{0.5})_{0.75}B_{0.2}Si_{0.05}]_{96}Nb_4$ BMG samples. Inset shows a magnified view of the serrated flow in the plastic regime of the CTC513K sample. (b) The values of σ_y and ε_p with error bars. (c) The shear band densities for the AC and CTC treated samples. Inset is the SEM image of lateral surface for the deformed CTC513K sample. (d) The relationship between σ_y and ε_p for typical Fe-based BMGs.

transition temperature, T_g) for 1 min, respectively. All the samples were treated for 15 cycles. The oil temperatures selected here are based on the consideration that the thermal temperature (room temperature) of CTC treatment locates in the range of 0.42–0.62T_g for La-, Zr-, ZrCu-based BMG systems in previous works [10–12]. The as-cast sample and those CTC treated samples at different oil temperatures are denoted as AC, CTC433K, CTC473K, CTC513K, CTC533K, and CTC563K samples, respectively. Compression tests were carried out using a Sans 5305 testing machine with a strain rate of $5 \times 10^{-4}\ s^{-1}$. The gage size of testing samples was 1 mm in diameter and 2 mm in length. Compression tests for each condition were conducted on 10 samples to ensure the reproducibility. The surface morphology of deformed samples before fracture was analyzed by scanning electron microscopy (SEM, Sirion 200, FEI). The thermal properties were examined by differential scanning calorimeter (DSC, Netzsch 404 F3) at a heating rate of 20 K/min. In order to measure the relaxation enthalpy (ΔH_{rel}), a second run under the same experimental settings was carried out right after the first heating process, and used as the baseline to be subtracted from the first DSC curve. 5 samples for each condition were tested to assess the reproducibility of ΔH_{rel} measurements. Microstructures of the samples were characterized by an X-ray diffractometer (XRD, D8-Discover, Bruker) with Cu-Kα radiation, synchrotron XRD, and aberration-corrected high-resolution transmission electron microscopy (HRTEM, FEI Titan 80–300). The samples for synchrotron XRD and HRTEM measurements were cut from identical rods to avoid the error caused by different casting conditions. The method based on the electron energy loss spectroscopy (EELS) was employed to measure the local thickness of the HRTEM samples [17].

Fig. 1(a) shows representative engineering stress-strain curves of the AC and CTC treated $[(Fe_{0.5}Co_{0.5})_{0.75}B_{0.2}Si_{0.05}]_{96}Nb_4$ BMG samples. The inset of Fig. 1(a) is a magnified view in the plastic regime of the CTC513K sample, clearly showing the serrated flow behavior of this sample. The values of σ_y and ε_p with error bars of these samples are plotted in Fig. 1(b). The large scatter of ε_p may originate from the presence of processing defects in samples and subtle difference of response to CTC treatment for each sample. Nevertheless, it is obvious that the ε_p increases with the increasing temperature from 433 to 513 K, then decreases with further increasing temperature to 533 and 563 K, while the σ_y maintains over 4000 MPa with CTC treatment. Among them, the CTC513K sample shows a significantly improved ε_p of 6.1%, combined with a high σ_y of 4060 MPa. The inset of Fig. 1(c) shows the lateral sur-

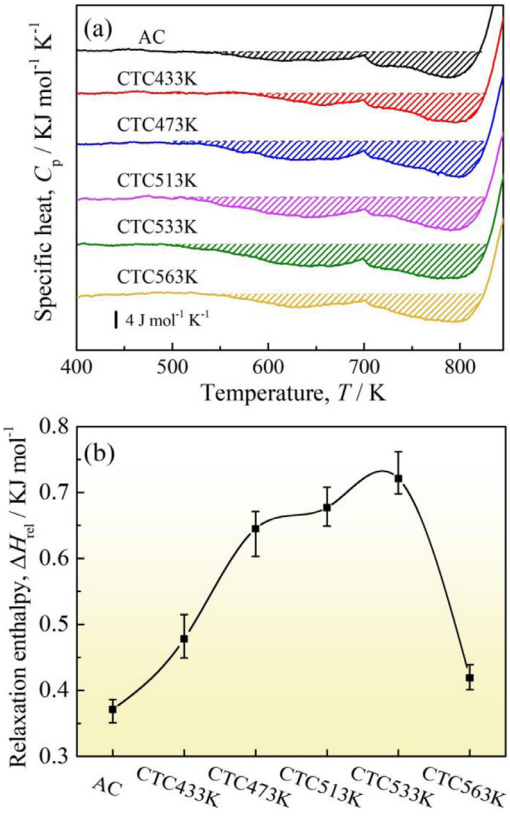

Fig. 2. (a) The relaxation spectra and (b) variation of ΔH_{rel} with error bars for the AC and CTC treated $[(Fe_{0.5}Co_{0.5})_{0.75}B_{0.2}Si_{0.05}]_{96}Nb_4$ BMG samples.

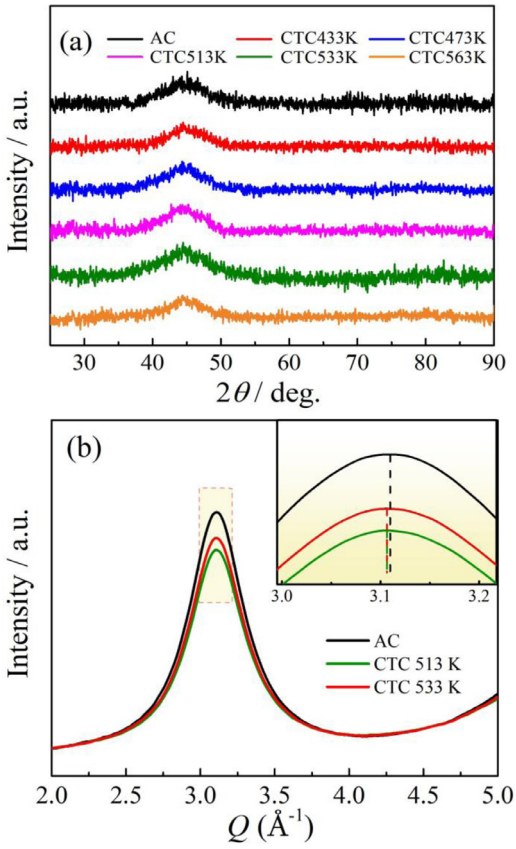

Fig. 3. (a) XRD patterns of the AC and CTC treated $[(Fe_{0.5}Co_{0.5})_{0.75}B_{0.2}Si_{0.05}]_{96}Nb_4$ BMG samples. (b) Synchrotron XRD patterns of AC, CTC513K, and CTC533K samples. Inset is the magnification image of the yellow rectangular area.

face morphology of the CTC513K sample unloaded prior to fracture. It is found that multiple shear bands (SBs) are formed, arrested and intersect with each other, resulting in the serrated flow behavior shown in the inset of Fig. 1(a) [18]. Furthermore, the shear band densities of the AC and CTC treated samples are calculated [19] and shown in Fig. 1(c). It shows that the shear band density increases with the thermal temperature increasing from 433 to 513 K, then decreases with further increasing thermal temperature to 533 and 563 K, indicating a positive correlation between the plasticity and shear band density. To compare the mechanical properties of this CTC treated $[(Fe_{0.5}Co_{0.5})_{0.75}B_{0.2}Si_{0.05}]_{96}Nb_4$ BMG with other typical Fe-based BMG systems, the data of σ_y and ε_p are summarized in Fig. 1(d) [5,18,20–33]. It is clearly seen that the CTC513K sample in this work shows a breakthrough in the general trade-off between plasticity and strength in the Fe-based BMG family. Based on the results mentioned above, the CTC treatment is an effective method to improve the plasticity of Fe-based BMG due to the increased density of SBs during deformation [34,35].

Fig. 2(a) shows the relaxation spectra of AC and CTC treated samples derived from DSC measurements, and the ΔH_{rel} is represented by the shaded area below the horizontal dashed line. The values of ΔH_{rel} for the samples are calculated, and their variation with the thermal temperature of CTC treatment is shown in Fig. 2(b). The ΔH_{rel} gradually increases with the temperature increasing from 433 to 533 K, and then decreases sharply for the CTC563K sample. The increased ΔH_{rel} is a sign of rejuvenation, which is acknowledged as the state of higher energy and more disordered structure, generally corresponds to the improved plasticity [36–38]. However, the CTC533K sample does not exhibit the largest ε_p although it shows the largest value of ΔH_{rel}. This inconsistence has also been reported by other researchers [10,12], indicating that the origins of structural changes affecting mechanical properties may not entirely be the same of those affecting the thermal behavior [39].

Therefore, further measurements were carried out to uncover the structural changes caused by CTC treatments at different settings. Fig. 3(a) shows XRD patterns of the AC and CTC samples of $[(Fe_{0.5}Co_{0.5})_{0.75}B_{0.2}Si_{0.05}]_{96}Nb_4$ BMG. As shown in the figure, all the samples keep amorphous structure. Fig. 3(b) shows synchrotron XRD patterns of the AC, CTC513K, and CTC533K samples. The curves of the three samples are smooth without sharp diffraction peaks, further confirming their amorphous nature. For clarity, the encircled part of the peak for the three samples was enlarged and shown in the inset, with the dashed lines denoting their peak positions (Q). The diffraction peak of the AC sample locates at the Q value of 3.110 Å^{-1}, and those of the CTC513K and CTC533K samples locate at the same Q value of 3.106 Å^{-1}. It has been proved that there is an inverse correlation between the diffraction peak position Q value and average interatomic spacing of metallic glass [40–42]. Thus, the decrease of Q values for the CTC513K and CTC533K samples indicates the increase in average interatomic spacing, which means that a more loosely packed structure is obtained in both samples through CTC treatment. Besides, the intensity of the diffraction peaks differs a lot, with the AC sample showing the sharpest diffraction peak, followed by the CTC533K and CTC513K samples. It means that the CTC513K sample has the highest degree of disordering, corresponding to the most rejuvenated structure. This may be the reason that CTC513K sample exhibits the best plastic deformation ability. The synchrotron XRD result is in line with the current understanding of structure-property relationships in BMGs that highly disordered

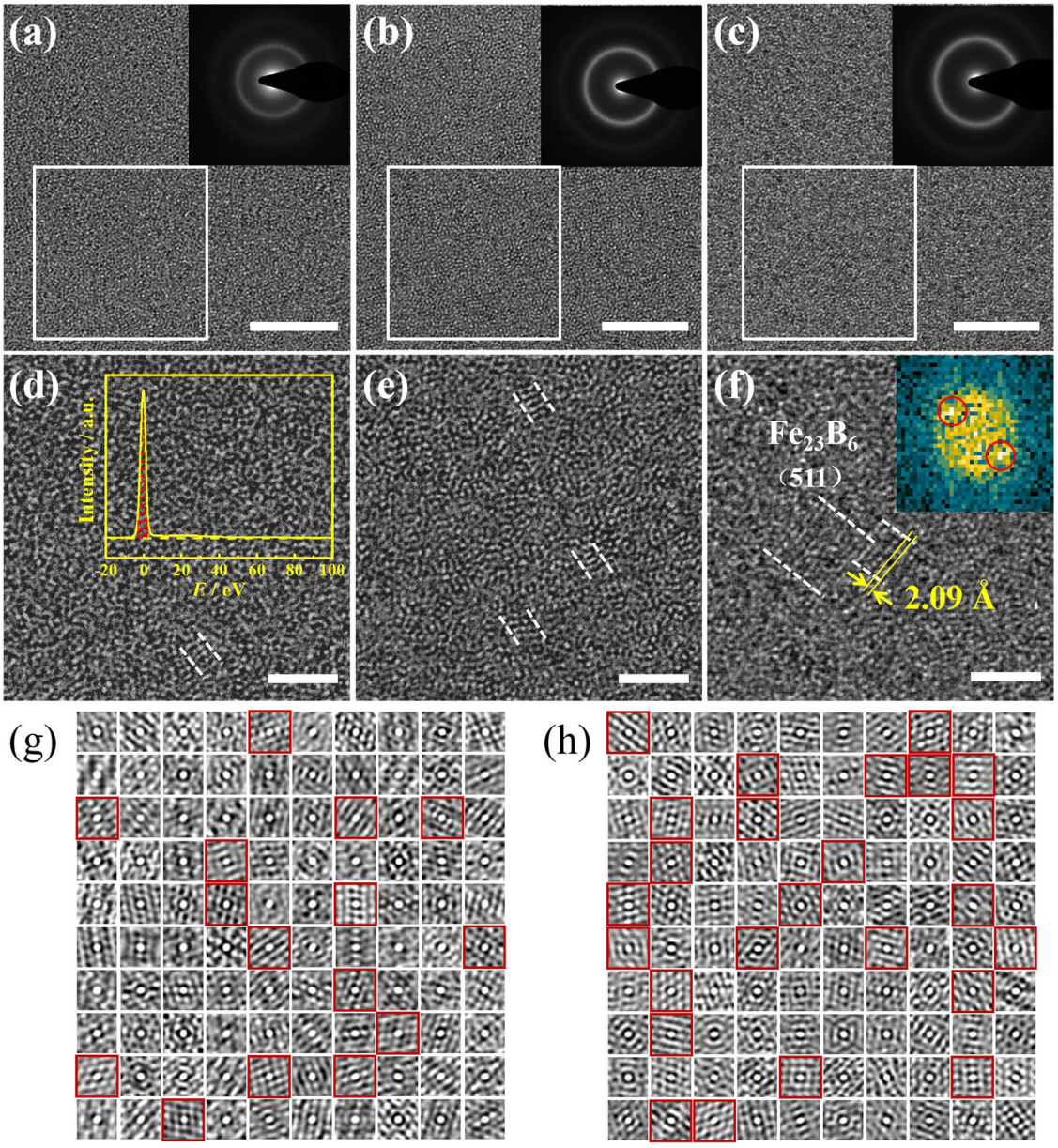

Fig. 4. The HRTEM images with the corresponding SAED patterns as insets for $[(Fe_{0.5}Co_{0.5})_{0.75}B_{0.2}Si_{0.05}]_{96}Nb_4$ BMG samples of (a) AC, (b) CTC513K, and (c) CTC533K. (d)-(f) The high magnification images of the areas highlighted by the white rectangles in (a), (b) and (c), respectively, with the dashed lines highlighting the CLO structures. The inset in (d) is the energy-loss spectrum from a 16 nm thickness region of the AC sample. (g)-(h) The representative 2D ACF of divided cells for the HRTEM images of (g) AC and (h) CTC513K. (scale bars, a, b and c - 5 nm, d, e and f - 2 nm).

glass generally behave in a ductile manner, and also indicates that there is pronounced structural change with CTC treatment.

To further investigate the atomic-scale structure change, the HRTEM observation was also conducted. Here, it is worth mentioning that the HRTEM images of all samples were captured at the regions with thickness around 15 nm, in order to reasonably compare the nano-crystalline precipitates in the three samples [32,43]. Fig. 4(a-c) show the HRTEM images and selected area electron diffraction (SAED) patterns of the AC, CTC513K, and CTC533K samples, respectively. As shown in the SAED patterns, there is no crystallization behavior in the samples before and after CTC treatment, which is consistent with the synchrotron XRD results. Fig. 4(d-f) are high magnification images of the regions highlighted by the white squares in (a), (b) and (c), respectively. The inset of Fig. 4(d) is the representative energy-loss spectrum of the AC sample. Based on the analysis of the zero-loss peak and a certain range of energy loss, the thickness of AC sample is estimated to be ~16 nm. The CTC513K, and CTC533K samples also show similar EELS results and have thickness around 15 nm. It is found that the atomic-scale ordering is different among the three samples. For the AC and CTC513K samples, some CLO structures with a size around 1 nm can be observed in the magnified images (Fig. 4(d, e)), which is characterized by a local fringe pattern reminiscence of translational symmetry. The average fringe spacing is around 2.00 ± 0.05 Å. It is interesting that the value does not correspond to FCC crystalline structure of $Fe_{23}B_6$ phase (distance of (511) lattice space: 2.07 Å), which is inclined to precipitate first in the (Fe,Co)-B-Si-Nb system [44,45]. For the CTC533K sample, some larger nanocrystals extending to 2–3 nm can be observed, as shown in Fig. 4(f). The Fast-Fourier-Transformation pattern (inset of Fig. 4(f)) of the area with lattice fringe shows clear diffraction spots, which confirms the existence of nanocrystals. As the average lattice fringe spacing of the

nanocrystals is measured to be 2.09 ± 0.05 Å, corresponding to lattice space of (511) of the $Fe_{23}B_6$ crystalline phase, it suggests that the nanocrystals in CTC533K sample are $Fe_{23}B_6$ crystalline phase. Besides, the areal fraction of CLO structures for the AC and CTC513K samples are calculated using the 2D autocorrelation function (ACF). The HRTEM images are divided into square cells with a size of 1.073 nm × 1.073 nm, which is close to the size of the observed CLO structure [43,46–47]. The details of the ACF analysis for 100 sub-images in two randomly selected regions of the two samples are elaborated in Figs. 4(g, h), respectively. The total fraction of CLO structures is 15% in the AC sample and increases to 25% in the CTC513K sample. The HRTEM results suggest that the CTC treatment can promote the formation of the CLO structure, and if the oil temperature is high enough, the CLO structure will grow into $Fe_{23}B_6$ crystalline phase. This evolution of atomic-scale structure may be induced by the internal stress, which is caused by the extreme temperature change of CTC treatment. During CTC treatment, the internal stress assists the atoms to hop from one sub-basin to another. As a result, some densely packed atoms can hop into the gulf and thus transform to a more ordered structure [48]. When the oil temperature is higher (over 533 K in our case), the evolution of the $Fe_{23}B_6$ crystalline phase occurs. It is worth mentioning that the HRTEM observation and the ACF analysis of the $[(Fe_{0.5}Co_{0.5})_{0.75}B_{0.2}Si_{0.05}]_{96}Nb_4$ BMG sample that only immersed into silicon oil at 563 K for 15 min (without thermal cycles) are also carried out (data not shown here). It is found that the total fraction of CLO structures after heating is only 17%, which is very close to 15% of the as-cast sample, indicating that the heating itself has no effect on crystal formation in this work.

Based on the results, the CTC treatment not only leads to rejuvenation in $[(Fe_{0.5}Co_{0.5})_{0.75}B_{0.2}Si_{0.05}]_{96}Nb_4$ BMG, but also brings to local ordering and crystallization. For the CTC513K sample, the enhanced plasticity is considered to be predominately originated from the higher structural rejuvenation degree and the increase of CLO density. Both the rejuvenated state and increasing number of CLO structures improve the nucleation of SBs [36,49]. And during the propagation of SBs, the previously formed SBs are subsequently hindered by the distributed CLO structures, which brings to the reactivation of new SBs [49,50]. As a result, the CTC513K sample shows abundant SBs during deformation. While for the CTC533K sample, some larger $Fe_{23}B_6$ crystalline ordering structures appear, which are hard and brittle. The $Fe_{23}B_6$ crystalline phase may increase stress concentration during compression test, leading to instantaneous catastrophic failure [51]. The results indicate that the effect of thermal cycling on mechanical properties of Fe-based BMGs is determined by the evolution of atomic-scale structure.

In summary, the CTC treatment is an effective method to affect the mechanical properties of $[(Fe_{0.5}Co_{0.5})_{0.75}B_{0.2}Si_{0.05}]_{96}Nb_4$ BMG by manipulating its atomic-scale structure. Through adjusting the thermal temperature during CTC treatment, the CTC513K BMG exhibits improved ε_p of 6.1%, combined with superhigh σ_y over 4000 MPa. The structure rejuvenation and increased local atomic-scale ordering induced by CTC treatment result in the enhancement of plasticity. Besides, the brittle crystalline structure is harmful to macroscopic plasticity, and should be avoided in the Fe-based BMGs. This work provides a fundamental guideline for designing Fe-based BMGs with large plasticity and high strength through CTC treatment.

Declaration of Competing Interest

The authors declare that they have no known competing financial interests or personal relationships that could have appeared to influence the work reported in this paper.

Acknowledgement

This work was supported by the National Natural Science Foundation of China (Grant Nos. 51631003 and 51871054), and the Fundamental Research Funds for the Central Universities (Grant Nos. 2242019k1G005 and 2242019K40183).

References

[1] A. Inoue, B.L. Shen, Adv. Mater. 16 (2004) 2189–2192.
[2] C. Suryanarayana, A. Inoue, Int. Mater. Rev. 58 (2013) 131–166.
[3] H.X. Li, Z.C. Lu, S.L. Wang, Y. Wu, Z.P. Lu, Prog. Mater. Sci. 103 (2019) 235–318.
[4] Q.J. Chen, J. Shen, D.L. Zhang, H.B. Fan, J.F. Sun, J. Mater. Res. 22 (2007) 358–363.
[5] K.F. Yao, C.Q. Zhang, Appl. Phys. Lett. 90 (2007) 061901.
[6] A. Makino, X. Li, K. Yubuta, C. Chang, T. Kubota, A. Inoue, Scr. Mater. 60 (2009) 277–280.
[7] S.F. Guo, L. Liu, N. Li, Y. Li, Scr. Mater. 62 (2010) 329–332.
[8] Y. Wu, H. Wang, X.J. Liu, X.H. Chen, X.D. Hui, Y. Zhang, Z.P. Lu, J. Mater. Sci. Technol. 30 (2014) 566–575.
[9] W.M. Yang, H.S. Liu, Y.C. Zhao, A. Inoue, K.M. Jiang, J.T. Huo, H.B. Ling, Q. Li, B.L. Shen, Sci. Rep. 4 (2014) 6233.
[10] S.V. Ketov, Y.H. Sun, S. Nachum, Z. Lu, A. Checchi, A.R. Beraldin, H.Y. Bai, W.H. Wang, D.V. Louzguine-Luzgin, M.A. Carpenter, A.L. Greer, Nature 524 (2015) 200–203.
[11] W. Guo, R. Yamada, J. Saida, Intermetallics 93 (2018) 141–147.
[12] W.L. Song, X.H. Meng, Y. Wu, D. Cao, H. Wang, X.J. Liu, X.Z. Wang, Z.P. Lu, Sci. Bull. 63 (2018) 840–844.
[13] H. Zheng, L. Zhu, S.S. Jiang, Y.G. Wang, F.G. Chen, J. Alloys Compd. 790 (2019) 529–535.
[14] S.V. Ketov, A.S. Trifonov, Y.P. Ivanov, A.Y. Churyumov, A.V. Lubenchenko, A.A. Batrakov, J. Jiang, D.V. Louzguine-Luzgin, J. Eckert, J. Orava, A.L. Greer, NPG Asia Mater. 10 (2018) 137–145.
[15] W. Guo, J. Saida, M. Zhao, S. Lü, S. Wu, Metall. Mater. Trans. A 50 (2019) 1125–1129.
[16] A. Inoue, B.L. Shen, C.T. Chang, Acta Mater. 52 (2004) 4093–4099.
[17] T. Malis, S.C. Cheng, R.F. Egerton, J. Electron Microsc. Tech. 8 (1988) 193–200.
[18] J. Zhou, B.A. Sun, Q.Q. Wang, Q.M. Yang, W.M. Yang, B.L. Shen, J. Alloys Compd. 783 (2019) 555–564.
[19] W.L. Ma, Y.L. Xu, B. Shi, J.G. Li, J. Mater. Sci. Technol. 33 (2017) 99–104.
[20] A. Inoue, T. Zhang, A. Takeuchi, Appl. Phys. Lett. 71 (1997) 464–466.
[21] K. Amiya, A. Urata, N. Nobuyuki, A. Inoue, Mater. Trans. 45 (2004) 1214–1218.
[22] Z.P. Lu, C.T. Liu, J.R. Thompson, W.D. Porter, Phys. Rev. Lett. 92 (2004) 245503.
[23] J. Shen, Q.J. Chen, J.F. Sun, H.B. Fan, G. Wang, Appl. Phys. Lett. 86 (2005) 151907.
[24] X.J. Gu, A.G. McDermott, S.J. Poon, G.J. Shiflet, Appl. Phys. Lett. 88 (2006) 211905.
[25] D.H. Kim, J.M. Park, D.H. Kim, W.T. Kim, J. Mater. Res. 22 (2007) 471–477.
[26] J.H. Yao, J.Q. Wang, Y. Li, Appl. Phys. Lett. 92 (2008) 251906.
[27] X.J. Gu, S.J. Poon, G.J. Shiflet, M. Widom, Acta Mater. 56 (2008) 88–94.
[28] Z.Y. Chang, X.M. Huang, L.Y. Chen, M.Y. Ge, Q.K. Jiang, X.P. Nie, J.Z. Jiang, Mater. Sci. Eng. A 517 (2009) 246–248.
[29] C.L. Zhao, C.C. Dun, Q.K. Man, B.L. Shen, Intermetallics 32 (2013) 408–412.
[30] S.F. Guo, J.L. Qiu, P. Yu, S.H. Xie, W. Chen, Appl. Phys. Lett. 105 (2014) 161901.
[31] P. Ramasamy, M. Stoica, S. Bera, M. Calin, J. Eckert, J. Alloys Compd. 707 (2017) 78–81.
[32] B. Sarac, Y.P. Ivanov, A. Chuvilin, T. Schöberl, M. Stoica, Z. Zhang, J. Eckert, Nat. Commun. 9 (2018) 1333.
[33] J. Zhou, Q.Q. Wang, X.D. Hui, Q.S. Zeng, Y.W. Xiong, K.B. Yin, B.A. Sun, L.T. Sun, M. Stoica, W.H. Wang, B.L. Shen, Mater. Des. 191 (2020) 108597.
[34] Z.F. Zhang, F.F. Wu, G. He, J. Eckert, J. Mater, Sci. Technol. 23 (2007) 747–767.
[35] B.A. Sun, W.H. Wang, Prog. Mater. Sci. 74 (2015) 211–307.
[36] A.L. Greer, Y.H. Sun, Philos. Mag. 96 (2016) 1643–1663.
[37] J. Pan, Y.X. Wang, Q. Guo, D. Zhang, A.L. Greer, Y. Li, Nat. Commun. 9 (2018) 560.
[38] L. Zhang, Y. Wu, S.D. Feng, W. Li, H.W. Zhang, H.M. Fu, H. Li, Z.W. Zhu, H.F. Zhang, J. Mater. Sci. Technol. 38 (2020) 73–79.
[39] J. Ketkaew, R. Yamada, H. Wang, D. Kuldinow, B.S. Schroers, W. Dmowski, T. Egami, J. Schroers, Acta Mater. 184 (2020) 100–108.
[40] A.R. Yavari, A.L. Moulec, A. Inoue, N. Nishiyama, N. Lupu, E. Matsubara, W.J. Botta, G. Vaughan, M.D. Michiel, Å. Kvick, Acta Mater. 53 (2005) 1611–1619.
[41] L.Y. Guo, X. Wang, K.C. Shen, K.B. Kim, S. Lan, X.L. Wang, W.M. Wang, J. Mater. Sci. Technol. 35 (2019) 118–126.
[42] F. Miao, Q.Q. Wang, Q.S. Zeng, L. Hou, T. Liang, Z.Q. Cui, B.L. Shen, J. Mater. Sci. Technol. 38 (2020) 107–118.
[43] Q. Wang, C.T. Liu, Y. Yang, J.B. Liu, Y.D. Dong, J. Lu, Sci. Rep. 4 (2014) 4648.
[44] A. Hirata, Y. Hirotsu, K. Amiya, N. Nishiyama, A. Inoue, Intermetallics 16 (2008) 491–497.
[45] A. Hirata, Y. Hirotsu, K. Amiya, N. Nishiyama, A. Inoue, Phys. Rev. B 80 (2009) 140201.
[46] X.J. Liu, G.L. Chen, H.Y. Hou, X. Hui, K.F. Yao, Z.P. Lu, C.T. Liu, Acta Mater. 56 (2008) 2760–2769.

[47] D. Cao, Y. Wu, H.X. Li, X.J. Liu, H. Wang, X.Z. Wang, Z.P. Lu, Intermetallics 99 (2018) 44–50.
[48] W. Guo, J.J. Saida, M. Zhao, S.L. Lu, S.S. Wu, J. Mater. Sci. 54 (2019) 8778–8785.
[49] F. Jiang, Y.L. Zhao, L.C. Zhang, S.B. Pan, Y.G. Zhou, L. He, J. Sun, Adv. Eng. Mater. 11 (2009) 374–379.
[50] L.Y. Chen, A.D. Setyawan, H. Kato, A. Inoue, G.Q. Zhang, J. Saida, X.D. Wang, Q.P. Cao, J.Z. Jiang, Scr. Mater. 59 (2008) 75–78.
[51] B.L. Shen, H. Men, A. Inoue, Appl. Phys. Lett. 89 (2006) 101915.